Marine Geology 369 (2015) 288–299

Contents lists available at ScienceDirect

Marine Geology

journal homepage: www.elsevier.com/locate/margeo

Shelf-to-canyon connections: Transport-related morphology and mass balance at the shallow-headed, rapidly aggrading Swatch of No Ground (Bay of Bengal)

Kimberly G. Rogers [a,*], Steven L. Goodbred Jr [a], Sirajur R. Khan [b]

[a] Department of Earth and Environmental Science, Vanderbilt University, PMB 351805, 2301 Vanderbilt Place, Nashville, TN 37235-1805, USA
[b] Geological Survey of Bangladesh, 153 Pioneer Road, Segunbagicha, Dhaka 1000, Bangladesh

ARTICLE INFO

Article history:
Received 4 January 2015
Received in revised form 12 September 2015
Accepted 20 September 2015
Available online 25 September 2015

Keywords:
Bay of Bengal
Ganges–Brahmaputra–Meghna Delta
Mass failures
Marine sediment transport
Clinoform deposition
Submarine canyon head

ABSTRACT

The Swatch of No Ground (SoNG) canyon in the Bay of Bengal is a shelf-incising submarine canyon that is actively aggrading in its upper reaches despite regular gravity-driven transport and mass wasting. Although the canyon lies 150 km downdrift of its main sediment source, the Ganges–Brahmaputra–Meghna (GBM) river mouth, high sedimentation rates (5–50 cm year^{-1}) are sustained by both progradation of the subaqueous delta into the canyon head and the conveyance of shelf-generated hyperpycnal flows to the canyon floor. This rapid accretion appears to be largely balanced by mass failures triggered by regularly occurring storms, and less frequently by major earthquakes. Here we use high-resolution sub-bottom sonar data to elucidate dominant sediment-dispersal pathways and their transport-related morphology at the canyon head; these include: 1) a laterally prograding clinoform that intersects the canyon head at water depths of 20–120 m; 2) several shelf-incising bypass gullies that originate in <20 m water depth above the rollover point and connect the inner shelf to the canyon floor, and 3) numerous U-shaped slide valleys formed by deep-seated mass failures initiating at water depths >50 m. The clinoform deposits reflect westward progradation of the GBM subaqueous delta into the upper canyon, where its axis-normal orientation leaves it dissected by cross-cutting gullies and mass failures. The morphology and acoustic stratigraphy of the gullies, coupled with strong bed shear and high suspended sediment concentrations on the inner shelf, suggest that these features are sustained by the regular conveyance of gravity-driven fluid muds that are formed in shallow water (<20 m) where the gullies originate. The downslope termination of the gullies coincides with a break in slope at the canyon floor, indicating that gullies serve as sediment conduits linking shallow water processes with sediment deposition in the lower canyon. Together these locally interacting shelf, clinoform, and canyon features form a unique composite morphodynamic system that more broadly defines the highstand connection between this large fluvial delta system and its shelf-indenting canyon.

1. Introduction

Submarine canyons are conduits for transporting terrigenous and marine material across continental margins and therefore play a significant role in the deep-sea preservation of climate and tectonic signals. Many of the world's modern submarine canyons are confined to the continental slope and are considered "headless" because they terminate on the slope with no apparent connection to a feeder channel. Other canyon systems extend further upslope, incising the shelf into shallow water depths of 20–150 m (Mullenbach and Nittrouer, 2000; Harris and Whiteway, 2011). Some modern examples of shelf-incising canyons connect to rivermouths where water and sediment may discharge directly into the canyon head, rapidly conveying fluvial sediment down-canyon (e.g., Sepik [Kuehl et al., 2004]; Congo [Savoye et al., 2009]). Other shelf-incising canyons have become separated from their source rivers during the Holocene transgression (e.g., Amazon [Milliman et al., 1975]; Danube [Popescu et al., 2004]). In these detached canyon systems, sediment and organic material are transported some distance from the river mouth across the shelf break or to the remote canyon head by currents or storm-related waves (Puig et al., 2004, 2014; Palanques et al., 2006).

Just as shelf-incising canyons can act as shelf bypass features that convey fluvial sediment directly from a river mouth to the deep sea (e.g., Sepik [Kineke et al., 2000]; Gaoping [Huh et al., 2009]), they can also serve as temporary storage sites for sediment and organic matter, until mass failure or erosion advect deposits further down-canyon (Puig et al., 2014). Down-slope transport events in shelf-incising canyons may result from a variety of circumstances, including: overburden

* Corresponding author at: Institute of Arctic and Alpine Research, University of Colorado, 4001 Discovery Drive, Boulder, CO 80303, USA.
E-mail address: kgrogers@colorado.edu (K.G. Rogers).

http://dx.doi.org/10.1016/j.margeo.2015.09.011
0025-3227/

pressure from increased or rapid sediment deposition, liquefaction caused by seismic activity or wave loading during storms, and over-steepening of canyon walls (Hampton et al., 1996; Mullenbach et al., 2004; Moscardelli et al., 2006; Talling, 2014). Thus, the frequency of mass wasting events is an important control on the rate at which sediments accumulating at a canyon head are remobilized further down-canyon or to the continental slope. Estimating sediment flux across the continental margin also depends on quantifying the balance of deposition and erosion at a canyon's head. However, documenting the mechanisms and rates of sediment transport into and out of a canyon head can be challenging (e.g., Monterey Canyon [Smith et al., 2005]). In shelf-incising canyons with high annual sediment deposition rates, such as the Swatch of No Ground canyon in the Bay of Bengal, accumulation must be balanced by export to maintain the stability and position of the canyon head through time.

The Swatch of No Ground (SoNG) (Fig. 1) is an example of a rapidly aggrading, shelf-incising canyon that connects to a modern fluvial system, one of only 153 such canyons out of 5849 mapped globally by Harris and Whiteway (2011). Although the SoNG canyon head is separated 150 km from its main sediment source (the Ganges–Brahmaputra–Meghna [GBM] river mouth estuary), aggradation rates up to 8 cm year^{-1} have persisted along the eastern Bengal shelf and upper canyon head since the mid-Holocene (Kuehl et al., 1989). As a consequence, frequent storms or major earthquakes that recur every 10–100 years have likely triggered the collapse and down-slope movement of overburdened sediments along the SoNG canyon head and inner Bengal shelf (Kudrass et al., 1998; Rogers and Goodbred, 2010; Palamenghi et al., 2011). At shorter-timescales, well-constrained ^{137}Cs and ^{210}Pb-derived accretion rates are 15–50 cm year^{-1} on the upper canyon floor (e.g., Kudrass et al., 1998; Michels et al., 2003), suggesting that the SoNG would have infilled within a few hundred years. However, the canyon head remains proximal to the modern shoreline just 30 km away. This circumstance suggests a quasi steady-state balance between sediment deposition and removal by mass wasting. This balance of sediment transport into and out of the SoNG canyon head, wherein high rates of deltaic deposition replace mass lost to wasting, define the longer-term behavior and evolution of the canyon.

Previous work on the SoNG and adjacent Bengal shelf has constrained sediment mass budget rates, stratigraphy, and event-scale impacts on the GBM subaqueous delta and upper SoNG canyon floor (e.g., Kuehl et al., 1989; Kudrass et al., 1998; Michels et al., 1998, 2003; Palamenghi et al., 2011), but these efforts did not extend to the uppermost canyon head where the system intersects the riverplume and its annual pulse of monsoon-discharged sediment. This is a critical juncture where high sediment concentrations and energetic shallow marine processes connect to a major canyon-slope-fan system. We present here evidence for three principal modes of sediment transport at the canyon head and discuss their apparent role in maintaining stability of the canyon head in a high-discharge shallow-marine environment. We also demonstrate that these modes of sediment exchange link shallow water deltaic processes to deep water canyon sediment transport, and place these features in an integrated sediment budget for the GBM delta system (Goodbred and Kuehl, 1999).

2. Oceanographic and geologic setting

Sediment and water discharge to the Bengal Basin are principally controlled by the Asian southwest monsoon (May–Sept), when the GBM sediment discharge system is an order of magnitude greater than during the dry season (Oct–Apr), ~ 992 × 10^6 tonnes and 93 × 10^6 tonnes, respectively (Coleman, 1969). Of the approximately one gigaton of annual sediment discharge, ~30% is deposited within the subaerial portion of the delta and adjacent coastal plain (Goodbred and Kuehl, 1998, 1999). The remaining 700 million tonnes discharged at the river mouth is partitioned among three primary depocenters: (1) the subaerial intertidal lower delta plain (Allison and Kepple, 2001; Rogers et al., 2013), (2) a rapidly prograding (15–20 m year^{-1}) subaqueous clinoform (Kuehl et al.,

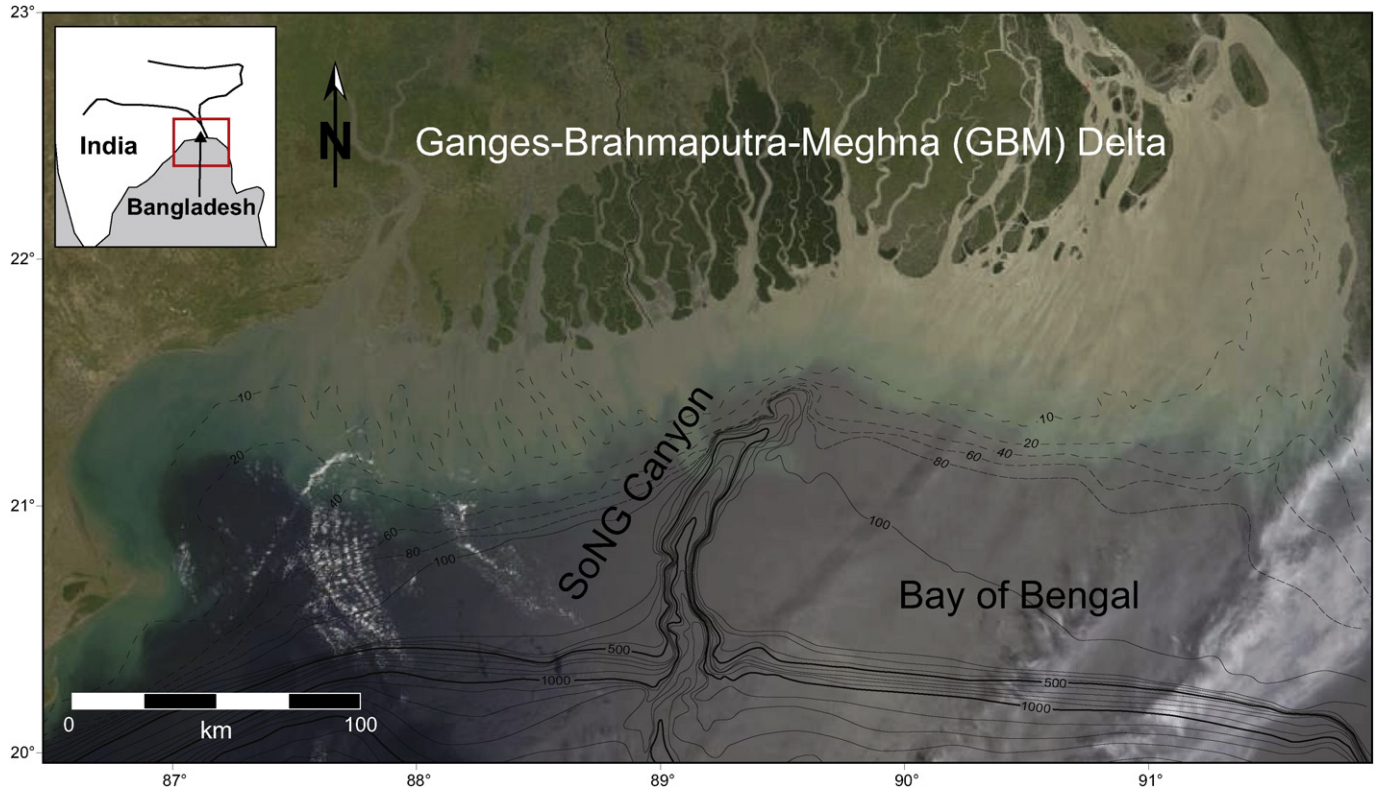

Fig. 1. MODIS image of the northern Bay of Bengal and bathymetry illustrating the proximity of the Swatch of No Ground canyon head to shore and to the subaqueous Ganges–Brahmaputra-Meghna delta. The clinoform topset–foreset rollover coincides with the seaward limit of the turbid water in the image. Bathymetric contours redrawn after Bangladesh nautical charts.

1997; Michels et al., 1998; Palamenghi et al., 2011), and (3) the SoNG canyon head (Michels et al., 2003).

2.1. The Swatch of No Ground and Bengal Fan

The Swatch of No Ground canyon incises the Bengal shelf in a NE–SW direction about 30 km offshore of the western coast of Bangladesh. The canyon deepens to >600 m within 60 km of the shore, and intersects the regional trend of the shelf break ~170 km from shore at 1200 m (at an average dip of ~0.6°). The modern canyon head lies ~150 km west of the river mouth, although onshore stratigraphy suggests that the Ganges and Brahmaputra rivers fed directly into the canyon in the early Holocene before avulsing to other portions of the delta after ~7000 years ago (Goodbred and Kuehl, 2000; Allison et al., 2003; Goodbred et al., 2014). The canyon continues across the shelf and upper slope for another 200 km where it connects to the upper Bengal Fan, earth's largest deep-sea fan (Sengupta et al., 1992; Weber et al., 1997). Unlike many modern canyon-fan systems associated with large rivers (e.g., Amazon [Flood et al., 1997]; Indus [Kolla and Coumes, 1987]; Mississippi [Kolla and Perlmutter, 1993]), the transfer of sediment from the upper SoNG to the Bengal Fan has remained active through the Holocene and into the modern. The presence of high ^{210}Pb and ^{137}Cs inventories on the fan channel-levee system indicate that large turbidity currents continue to originate from the upper canyon (Weber et al., 1997; Hübscher et al., 1998), which we speculatively link with observations of storm-induced sediment remobilization and mass failure at the canyon head (Kudrass et al., 1998; Rogers and Goodbred, 2010).

2.2. Upper canyon sedimentation

The rollover point from the low-gradient inner shelf into the canyon head occurs at ~20 m water depth, where the eastern margin of the canyon head intersects the prograding subaqueous delta foresets. Sedimentation rates of 5–7 cm year^{-1} along the eastern rim of the canyon are equivalent to rates of accumulation on the deltaic clinoform foresets at mid-shelf (Kuehl et al., 1997; Fig. 2). By contrast, ^{137}Cs dating of graded sand and silt layers alternating with finely laminated muds on the canyon floor reveal much higher accumulation rates of 45–50 cm year^{-1} (Kudrass et al., 1998). These extremely high rates are attributed to the combination of westward transport of coarse silt and sand eroded from the clinoform topsets during vigorous storm events and deposition of "quasi-continuous" sediment gravity flows driven by currents generated during high discharge (Sengupta et al., 1992; Barua et al., 1994; Kudrass et al., 1998; Kottke et al., 2003; Michels et al., 2003). Based on these rates, it is thought that the canyon intercepts up to 30% of the total sediment load discharged at the GBM river mouth (Kuehl et al., 1989; Michels et al., 1998). Water-column data from the inner shelf taken by Barua et al. (1994) indicates along-shore depth-averaged suspended sediment concentration (SSC) is significantly higher during maximum discharge (4–6 g l^{-1}) than in the dry season (0.1–1.5 g l^{-1}). Such seasonally elevated SSC combined with strong wave and tidal bed shear on the inner shelf suggests that the SSC near the bed can easily reach that required to form a hyperpycnal fluid mud (>5 g l^{-1}) during high discharge (Barua et al., 1994). Indeed, the ratio of sediment discharge at the rivermouth to the volume of inner-shelf waters (5–20 m deep) yields a mean SSC of ~2 g l^{-1}. Because annual sediment accretion on the inner shelf and adjacent tidal deltaplain (~100 × 10^6 tonnes year^{-1}, each; c.f.

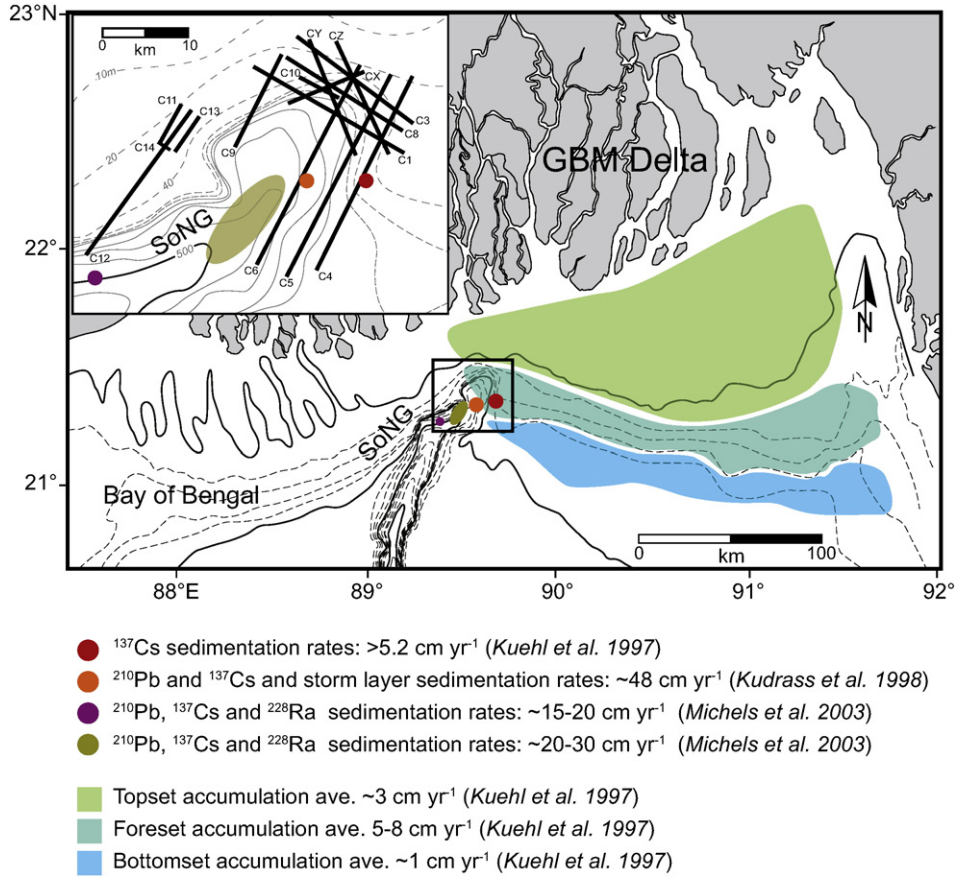

Fig. 2. Measured sedimentation rates across the Bengal shelf, clinoform and in the Swatch of No Ground Canyon. Annually averaged sedimentation rates are highest on the clinoform foresets and at the eastern canyon head. Inset shows upper canyon head bathymetry; black lines labeled C1 to C14 and CX, CY and CZ are sonar track lines used in this study. Note that maps in subsequent figures may not include all sonar lines.

Kuehl et al., 1997; Rogers et al., 2013) can only account for ~40% of this material, it is required that river-sediment discharge be regularly conveyed to the foreset and upper canyon depocenters.

3. Methods

High-resolution sub-bottom CHiRP sonar data were collected over a 400-km^2 area at the Swatch of No Ground canyon head and adjacent inner Bengal shelf in March 2007 and March 2008. The surveys were collected using a shallow-towed (~10 m above the seafloor) Edgetech 216s chirp system operated at a 2–10 kHz frequency collected at an average speed of 7 knots. This high frequency acquisition system images the uppermost <80 ms TWT (~60 m) of the sub-seafloor, and has a vertical resolution of <1 m in unconsolidated fine-grained sediment. Depth conversions for the sonar data assumed a mean sound velocity of 1500 m s^{-1} with no application of a velocity profile given the shallow penetration depths. A 5% velocity difference at 60 m penetration is equivalent to a depth error of ±3 m.

Data collection in 2007 included ~200 km of the Bengal Shelf and canyon head in water depths of 20–500 m below sea level (mbsl). This includes the topsets and foresets of the subaqueous clinoform. The 2008 survey traced the same canyon survey lines of 2007 but included an additional 150 km of data in order to expand coverage of the uppermost canyon. The sonar lines principally used in this study include eight NE–SW trending along-canyon lines and six NW–SE trending cross-canyon lines (Fig. 2). Raw sonar data was converted to a seg-y format using the Edgetech Discover v. 3.3 acquisition program. The seg-y files were processed using Triton Sub-bottom Interpreter software and then exported into Fledermaus IVS 3D for simulated three-dimensional viewing. Although the sonar lines strike the canyon head NW–SE (cross-canyon) or NE–SW (along-canyon), cardinal directions are principally used in this paper to describe the position of transport-related features.

4. Results

Acoustic penetration within the upper-canyon deposits ranged 10–50 m below the seabed, typically 20–30 m, with differences controlled by depth of the seabed multiple, shallow gas, or attenuation of the signal. Radiometric dating of the sedimentary deposits in these areas demonstrate accretion rates of 5–8 cm year^{-1} around the canyon rim with rates increasing to 15 cm year^{-1} across the canyon margin and to >30 cm year^{-1} on the upper canyon floor (Kuehl et al., 1997; Kottke et al., 2003; Michels et al., 2003). At these rates the 10–50 m of strata imaged in the dataset represent only the last 200–1000 years of sediment deposition. Thus, acoustic reflectors observed at the ~10-cm resolution of this 2–10 kHz sonar dataset reflect time intervals <10 years, perhaps locally revealing annual bedding in areas of higher accumulation. Regardless of the exact time interval, these acoustic data are capturing decadal to sub-decadal processes that have been operating over the last few hundred years since present.

The overarching morpho-acoustic attribute of the sonar dataset around the canyon head is parallel to subparallel acoustic reflectors that are traceable over distances of kilometers from the inner shelf into the canyon (Figs. 3 and 4). This pattern of regular acoustic bedding corresponds with upward fining depositional packages observed in other parts of the canyon that are attributed to spring-neap tidal cycles, seasonal variations in discharge, and suspension settling of storm-generated sediment plumes (Kudrass et al., 1998; Michels et al., 2003). These acoustic characteristics of sedimentary deposits in <200 m water depth at the canyon head are similar to those described for the middle canyon (i.e., 200–600 mbsl) (e.g., Kottke et al., 2003). However, an important distinction is that the prevalent parallel to subparallel acoustic reflectors are intensely disturbed in many areas of the uppermost shallow canyon head, with deformed bedding and structural features, including growth faults, buried slumps, fluid escape structures, and acoustically transparent units characteristic of sediment liquefaction (Figs. 3 and 4).

4.1. Depositional features — clinoform development

Since the slowdown of sea level rise in the mid Holocene (~7 ka), sediment discharge onto the Bengal shelf has supported subaqueous delta progradation across the shelf at rates of 15–20 m year^{-1} (Kuehl et al., 1997; Hübscher et al., 1998). On the eastern shelf, well-stratified beds oriented parallel to the canyon's eastern edge are an extension of the deltaic clinoform and can be traced laterally for ~20 km before thinning and downlapping onto a transgressive ravinement of the lowstand exposure surface at 80–100 mbsl in the east and deepening to >100 m at SoNG margin (Fig. 3A; Michels et al., 1998; Palamenghi et al., 2011). It is here that the deltaic clinoform intersects the SoNG, where it progrades into the canyon head and has deposited at least 50 m of finely (<1 m) stratified, parallel to sub-parallel bedding along the canyon's eastern flank (sonar lines C4, C5, and C6; Figs. 3A and 4). These clinoform strata dip into the canyon at 2–3° and are observed to drape topographic irregularities such as acoustically transparent layers, faults and glide planes for slumps. This draping of stratified sediment over irregular sub-bottom features indicates that many of these disturbances originally formed at the seabed and have since been buried by continued clinoform deposition. Other stratified sediments from disturbed areas of the clinoform show vertically increasing depth offsets that reflect the persistence of growth faulting through time (Fig. 3A).

Deposition in the canyon head is also characterized by sigmoidal clinoform units up to 6 m thick that extend across the canyon head normal to the canyon's downslope axis. These units can be continuously traced from the inner shelf (0.2°) into the canyon, where they steepen (2–3°) and extend nearly to the opposing western canyon margin (Figs. 3B and 4). The main difference between this axis-normal clinoform development (i.e., northern canyon boundary) and the canyon-parallel progradation (i.e., eastern canyon margin) is that the axis-normal clinoform is more frequently punctuated by growth faults, thick (<20 m) transparent layers, buried slumps, and chaotic and concave bedding (Figs. 3B and 4). These irregular features are related to sediment instability and failures, which often occur in vertically stacked successions that are separated by several meters of acoustically stratified sediment reflecting deposition between disturbance events (Fig. 5).

4.2. Erosional features — mass failures

Interrupting the pattern of clinoform growth and rapid sedimentation in the upper canyon are prevalent mass failures, deformed bedding, and related slip planes and growth faults. These features can be generally categorized into two principal types of erosion-related failures: 1) sequences of buried acoustically transparent sedimentary units separated by parallel bedding contiguous with up-dip clinoform strata, and 2) wide (<2 km) valleys at the seabed with acoustically transparent material at their floors atop contorted beds visible in the deeper subsurface (Fig. 5). For these latter features, the U-shaped valley systems and their episodic evacuation were documented following the passage of Cyclone Sidr in 2007 and described in detail by Rogers and Goodbred (2010). In this subsequent paper, we further explore the history of these features in the acoustic record and place their distribution and role in context of the broader shelf-canyon transport system.

The acoustically transparent layers lack coherent bedding structures and are recognized to form through sediment displacement by mass flows or in situ liquefaction with local displacement (e.g., Prior et al., 1986; Trincardi et al., 2004; Palamenghi et al., 2011; Rogers and Goodbred, 2010). In the SoNG canyon head, up to three sets of these transparent units (<10 m in thickness) are present in the subsurface and found interspersed with acoustically stratified units (T1, T2 and T3 in Fig. 5). Each set of transparent layers has irregular, wavy upper

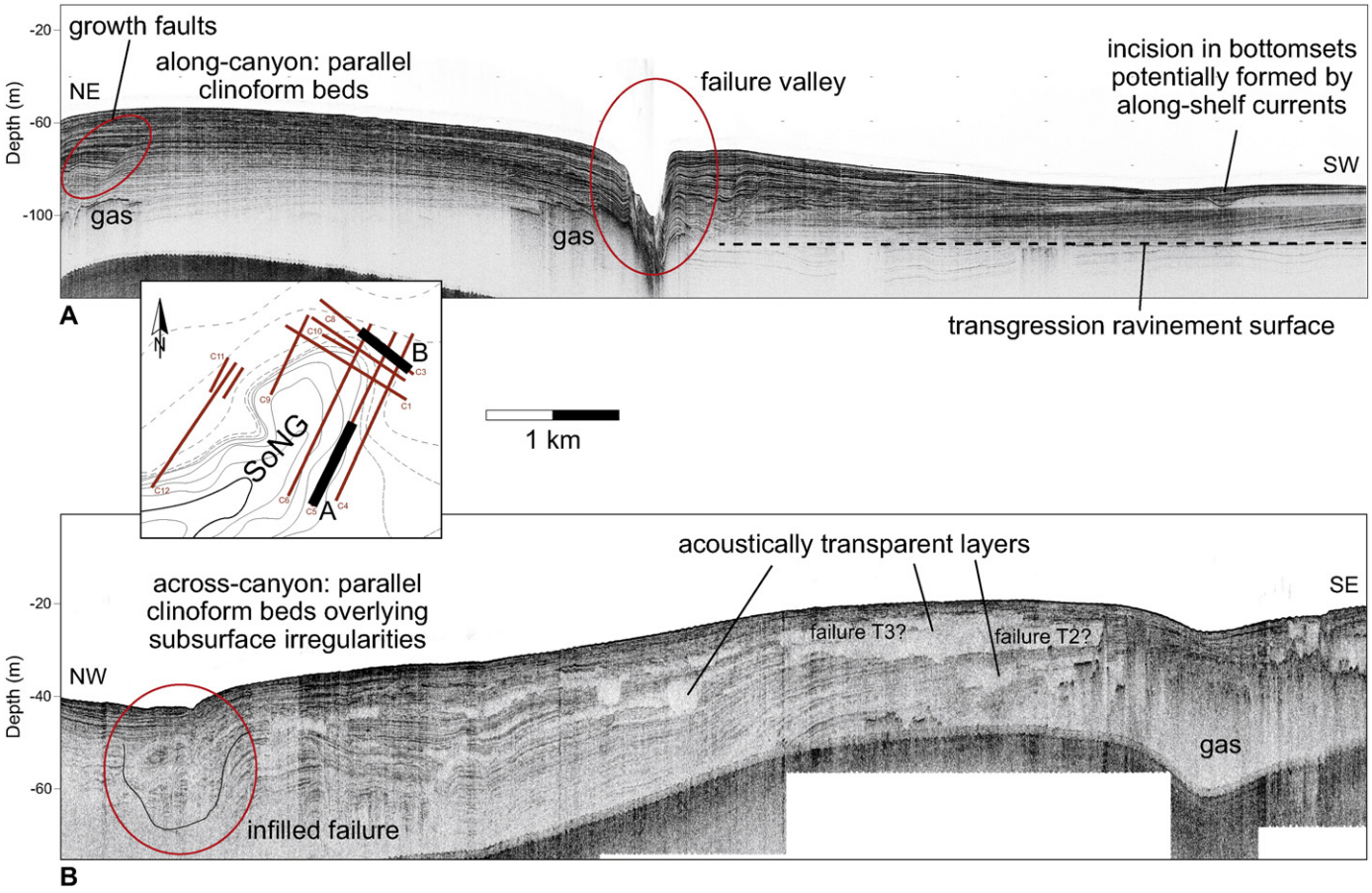

Fig. 3. A. Along-canyon section of chirp sonar line showing the profile of the Holocene clinoform prograding onto a transgressive erosional surface. Incising the clinoform is a valley potentially formed through sediment collapse during a storm or from rapid sediment loading. B. Cross-canyon line showing parallel, well-stratified beds indicative of the clinoform. Irregularities such as slumps and acoustically transparent layers are visible in the subsurface. Pockets of subsurface gas are evident in both lines and appear as acoustically opaque layers with flat tops. Locations of the sonar line sections shown in A and B are indicated on the inset map with a bold line.

and lower boundaries that conform to the underlying topography and are generally truncated on either side by low-angle walls that locally contain the failure sequences. Draping strata in between each transparent layer can be traced up-dip onto the shelf and are laterally contiguous with clinoform bedding, indicating that deltaic sedimentation resumes at the canyon head following failure events.

The relative age of the three failure-sedimentation sequences is estimated by comparing the top depth of each transparent layer in Fig. 5 to sedimentation rates of 5 to 15 cm year^{-1} determined through ^{137}Cs and ^{210}Pb-dating of cores collected in the SoNG at this location (Fig. 2; Kuehl et al., 1997; Kudrass et al., 1998). The tops of units T1, T2 and T3 are buried ~40, ~20 and ~15 m below the seabed, and correspond to 800 to 266, 400 to 133, and 300 to 100 years, respectively. This demonstrates that disturbances to upper SoNG stratigraphy recur on relatively short time scales (i.e., <1000 years) and highlights the apparent balance between rapid sediment aggradation and recurring mass failures in modulating the mass balance of sediment into and out of the canyon head and sustaining the relatively uniform position of the SoNG canyon head.

4.3. Bypass features: gully system

Submarine gullies are described as shallow (1 to 20 m) channel-like features of varying width, typically a few hundred meters, that are widely found in continental slope, canyon and deltaic settings (e.g., Atlantic margin [Twichell and Roberts, 1982]; Rhône River prodelta [Maillet et al., 2006]; Northern California slope [Spinelli and Field, 2001]). They generally initiate through erosion by gravity flows (Izumi, 2004), although features of similar scale may also originate through vertical deposition and construction (e.g., Straub and Mohrig, 2009). Once established, gullies morphodynamically evolve to serve as sediment-bypass features that primarily convey gravity currents from shallow water environments to deeper-water depocenters. In the northern SoNG canyon head, at least two such gully systems are found to cross-cut the erosional and depositional features described in Sections 4.1 and 4.2. Other broadly similar features deeper in the canyon (>300 mbsl) have been identified and labeled as "gullies" by Kottke et al. (2003); however, these are dimensionally much larger (i.e., >1 km wide by >300 m deep) and more closely resemble the failure valleys described for the upper canyon head. Rather, the two shallow-water gully systems originate on the inner shelf near the topset–foreset rollover and traverse the accreting canyon clinoform to the canyon floor at ~200 m water depth; one of gully systems is oriented NE–SW and the other N–S (Fig. 6).

Each gully shares similar attributes: steep-sided walls (7–10°); shallow water (<20 mbsl) origins; thalweg slopes of 1°, and are traceable for up to 10 km across the canyon-infilling clinoform onto the canyon floor (Table 1). Although the gullies maintain their general shape and width over their length, the water depth to the tops of the gullies progressively deepens down-canyon. The maximum relief of the gullies (from top to base) is ~20 m and occurs where thickness of the clinoform is greatest (Fig. 7). At such locations, the gully form is traceable deeper in the subsurface indicating that these features are locally persistent and aggrade vertically with clinoform deposition, not unlike the constructional canyon features described by Straub and Mohrig (2009).

Although persistent at a given location, the gullies do show evidence for lateral migration, whereby truncated and downlapping strata occur

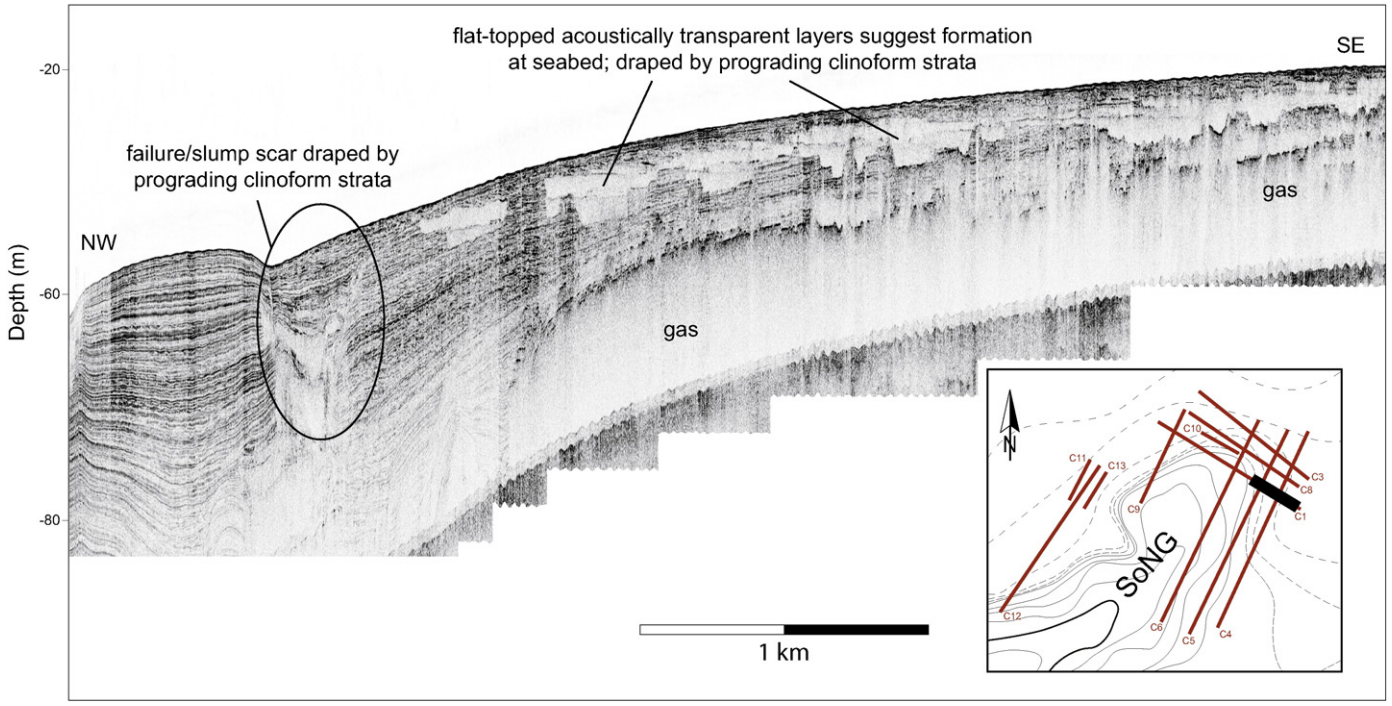

Fig. 4. Example of western edge of the clinoform prograding into the canyon head. Finely laminated, thin-bedded strata persist across the inner shelf in water depths of ~20 m. At the edge of the canyon, the slope of the seabed increases, and stratal layers thicken and bend towards the center of the canyon. Clinoform strata contain acoustically transparent layers with flat tops interpreted as mudflows formed at the seabed from storms, or from internal liquefaction during earthquakes. Internal slumping appears as transparent sections infilled by parallel strata that drape the subsurface irregularities, suggesting that progradation resumes after failure occurs. Location of the sonar line section is indicated on the inset map with a bold line.

on opposing gully walls (Fig. 7). Most commonly, the downlapping strata occur along the gully wall lying updrift of the advancing clinoform. This non-uniform deposition results in an asymmetric gully form with downlapping strata dipping at an angle 1–3° less than the opposite wall (Table 1). The strata along the steeper gully walls are consistently truncated by erosion where they oppose areas experiencing clinoform deposition, demonstrating that the gully form migrates laterally as the updrift wall preferentially accumulates clinoform sediment (Fig. 7). This lateral migration, however, appears to be relatively slow compared with the fast pace of vertical aggradation, with a roughly 2:1 ratio of horizontal:vertical translation for the gully form (c.f. fluvial channels >100:1; Gibling, 2006).

5. Discussion

Several modes of sediment transport, involving deposition, erosion, and bypass, are represented by the major geomorphic features around the SoNG canyon head. The clinoform, mass failures and gullies are all collocated, each overprinting one another within the ~100 km^2 area of the canyon head shallower than 200 m water depth (Fig. 8). The consistent morphology and coherent distribution of these features provide valuable insight into the transport processes operating at the canyon head, even though no study has yet observed the discrete physical mechanics involved. Nevertheless, considerable constraint on their interpretation is provided by numerous studies of the adjacent Bengal shelf and deeper parts of the SoNG canyon (Barua, 1990; Barua et al., 1994; Kuehl et al., 1989, 1997; Kudrass et al., 1998; Michels et al, 1998, 2003; Kottke et al., 2003, Palamenghi et al., 2011).

5.1. Seasonal mechanisms for sediment delivery: fluid mud formation

The lack of deformation in the acoustic reflectors that define the gully systems and their recent history indicate that these features have been relatively stable and resisted failure despite recurring storms in the Bay of Bengal. These attributes are consistent with the gullies being formed and maintained through the regular conveyance of gravity-driven sediment flows, or fluid muds, apparently sourced from the inner shelf where the gullies originate. Downslope migration of fluid muds was first described as an episodic transport phenomenon triggered by wave- and current-generated boundary shear stresses on the subaqueous Amazon delta (Sternberg et al., 1996). Fluid muds have since been documented in nearly all fluvial-marine shelf settings where suspended sediment concentrations are high and waves or tidal currents are energetic (Wright and Friedrichs, 2006). Where such river discharge is proximal to shelf-incising canyons, fluid muds generated on the shelf may also be conveyed into the canyon system. On the Fly River subaqueous clinoform in Papua New Guinea, fluid mud gravity flows are transported across the clinoform in channels near the river mouth where tidal energy exceeds 1 m s^{-1} (Harris et al., 1993). Similarly, the focusing of storm waves around a canyon head's, such as the Eel River canyon, can concentrate near-bottom suspended sediment that is then episodically mobilized into the canyon (Puig et al., 2004).

Though rheological measurements of fluid mud are difficult to make in situ (e.g., Kineke et al., 1996), we can constrain the likelihood of fluid mud formation and funneling to the interior of the SoNG canyon via the gully systems based on their morphology and the hydrodynamics of the Bengal shelf. For the latter, high SSC of the GBM floodpulse (depth averaged 4–6 g l^{-1}), strong tidal pumping (open-shelf velocities >1 m s^{-1}), high storm frequency (avg 1.5–2 $year^{-1}$) and wave regime (avg. wave heights <4 m) are widely present on the Bengal shelf and together reflect conditions ideally suited for fluid mud development (Islam et al., 2002; Barua et al., 1994; Alam et al., 2003). Furthermore, the heading of SoNG gullies in shallow water near the topset–foreset rollover (<20 m) also suggests that they convey flows originating on the inner shelf where wave- or tide-supported sediment gravity flows regularly develop (Wright and Friedrichs, 2006). Once generated on the surrounding inner shelf, we suggest that fluid muds accelerate at the canyon rollover (~20 m depth) and are captured by the gully systems and conveyed to the principal canyon thalweg that actively feeds the upper Bengal fan (Michels et al., 2003). With time, the SoNG gully

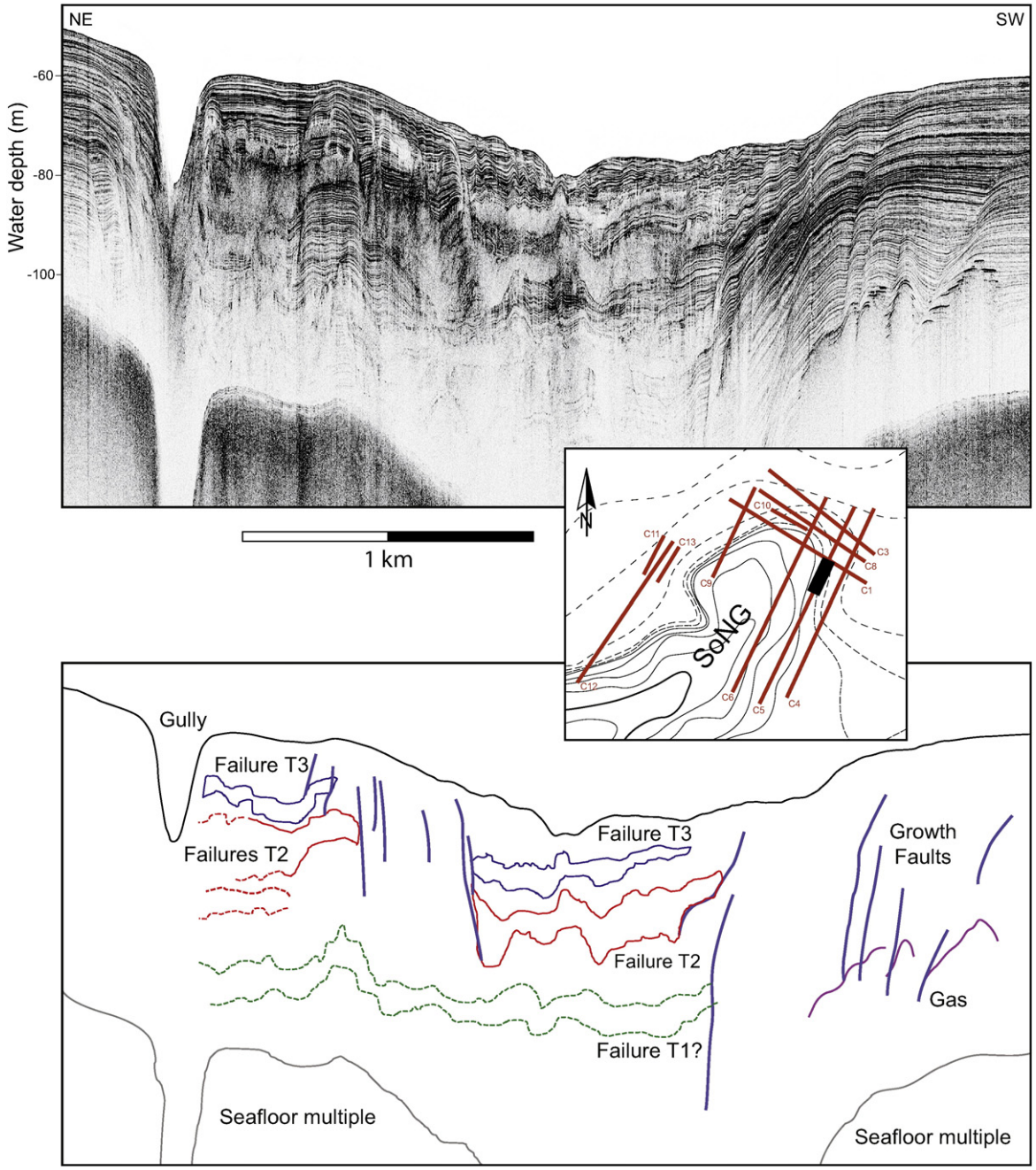

Fig. 5. Fragment of chirp sonar line C5 and interpreted section showing at least three failure events (T1, T2, T3) separated by parallel strata contiguous with clinoform beds up-dip. Location of sonar line fragment is indicated on the inset map with a bold line.

forms aggrade either through the overflow of gravity currents moving through them or clinoform growth and settling of plume sediment. Nevertheless, the apparent regular conveyance of sediment gravity flows through the gullies likely prevents the gullies from infilling by this rapid background deposition associated with the riverplume and clinoform growth (Michels et al., 2003).

5.2. Eastern vs. western canyon failures

Across the canyon, there is a distinct transition in the type of failure valleys that occur along the margins, from smooth-floored failure valleys in the east and north (i.e., SV-3 and SV-4, Fig. 6) to blockier valley floors downdip and to the west (i.e., SV-1, SV-2, Fig. 6 and WSV-5, Fig. 9). Given the considerably different sediment accretion rates in these areas, we attribute the different failure styles to differences in the consolidation of pre-failure strata at these locations. Annual decimeter-scale sedimentation rates along the eastern and northern canyon head result in rapidly buried, underconsolidated and overpressured sediment that is more susceptible to fluidization and failure as turbidity currents; in contrast, older and/or more slowly accreting deposits in the west and down-canyon are presumed to be more consolidated, with higher internal shear strength and a pattern of failure as a debris flow of semi-coherent blocks (e.g., Hampton et al., 1996; Syvitski et al., 1987).

Consistent with these interpretations, the western canyon-head margin is considerably steeper than those along eastern and northern sides (~10° versus 2–3°), suggesting that the western canyon margin is largely relict, with limited accretion over the past several hundred years (i.e., the time frame of actively accreting features described here). During Cyclone Sidr, an existing valley system along the western

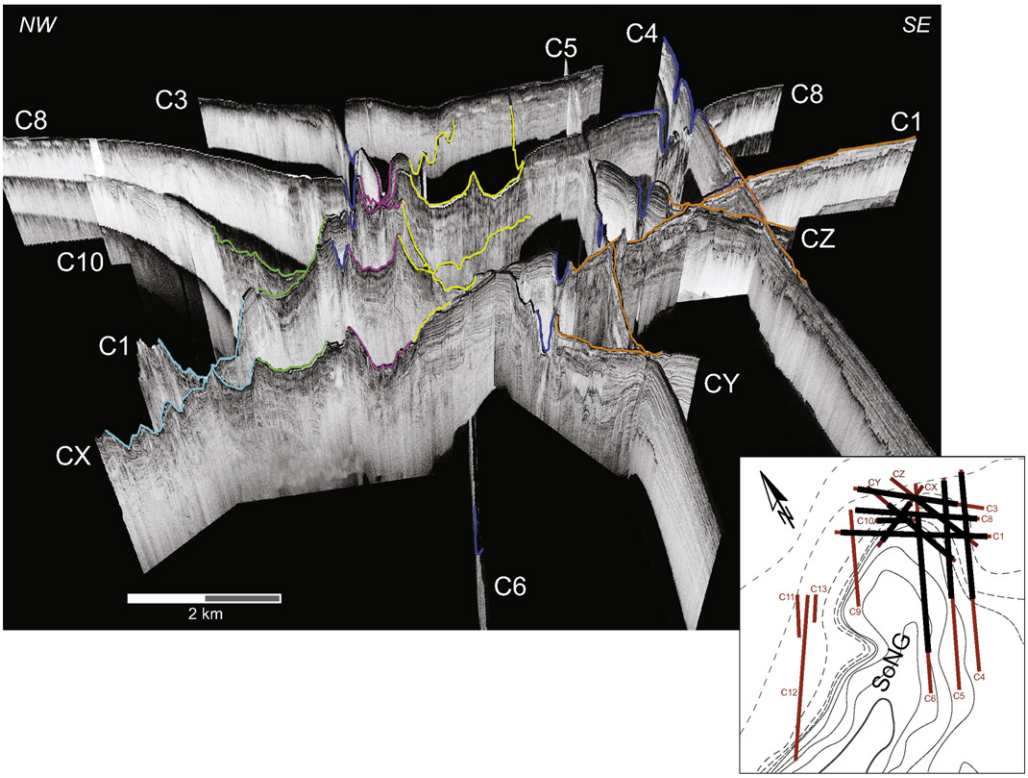

Fig. 6. Fledermaus fence image highlighting the four main valley systems created in the SoNG canyon head following Cyclone Sidr, and the resistant gully features. Failures were identified as segments of discrete valley systems by rotating and examining sonar lines in 3D space using Fledermaus and aligning adjacent valley edges. The discrete valley systems are identified in this image by color coding of the four main valley systems from west to east: SV-1 (cyan); SV-2 (green); SV-3 (pink), and SV-4 (yellow). The lowermost down-canyon sonar line (C1 and SW edge of CX) contains a blocky-floored feature that aligns with at least three of the valleys (i.e., SV-2, -3 and -4). The position of this section in the southwest side of the canyon head is consistent with the orientation of the main canyon thalweg, and may represent the upper-most preferred flow pathway for sediment transport originating in the canyon head. The gully systems are highlighted in dark blue. Locations of sonar line sections are indicated on the inset map with bold lines.

canyon rim experienced a major head-cutting failure that extended the valley at least 1 km upslope onto the shallow western shelf (WSV-5, Fig. 9). This large failure was captured in the western-most boundary of the dataset, revealing that headward extension of the canyon does occur, but apparently only where such failures are not offset by subsequent deposition such as they are along the actively accreting eastern margin.

5.3. GBM sediment budget and canyon head stability

The ~700 × 10^6 tonnes of sediment annually discharged at the GBM rivermouth is partitioned between the rapidly prograding subaqueous delta (~400 × 10^6 tonnes), the "abandoned" tidal delta plain (~100 × 10^6 tonnes) and the canyon (~200 × 10^6 tonnes) (Kuehl et al., 1997; Allison, 1998; Rogers et al., 2013). The proximity of the SoNG to the river mouth (~150 km) has sustained high rates of sedimentation at the canyon head (5–10 cm $year^{-1}$). At these rates, the shallow shelf around the canyon head (~20 mbsl) should have filled to sea level in less than 1 kyear (Kuehl et al., 1989). Since this has not happened, sediment must be removed to prevent infilling of the canyon head. Failures such as those documented in this paper and in Rogers and Goodbred (2010) provide an effective mechanism for removing large volumes of sediment from the canyon head to the inner canyon and potentially the Bengal Fan.

To place the recent cyclone-induced failures in context of the overall GBM sediment budget, the minimum volume of material displaced in the upper canyon head was calculated from the summed changes in cross-sectional area between pre- and post-storm 2D sonar lines (Table 2). Each segment of the U-shaped failure valley is conceptualized here as an ellipse with the long axis in the strike (E–W) direction, since the widths of the failure valleys measured in the 2D sonar lines are an average of ~50 times wider than their depths (Table 2). A modified equation for ellipse area was used to calculate the total for the five main failure valleys and two additional failures. The volume of material displaced in each valley segment of the failure valleys was then calculated using:

$$[((\pi AB) / 2) * L] * \rho$$

where A is the half width (m) of each failure valley, B is the average thickness (m) of material removed in each failure, L is the distance (m) between the failure and the next closest down-canyon sonar line, and ρ is the dry bulk density of sediment deposited in the canyon head, taken as 1.5 (g cm^{-3}) (per Michels et al., 2003). The total volume

Table 1
Characteristics of gully systems.

Gully system	Estimated runout length (m)	Slope of gully system thalweg (°)	Avg width of gully (m)	Water depth to top of gully (m)	Avg depth of gully from seabed (m)	Wall angle (°)
Northern	4900	2–3	206 ± 55	20–120	19 ± 2	12–13
Eastern	10,000	2–3	250 ± 51	20–150	21 ± 6	13–16

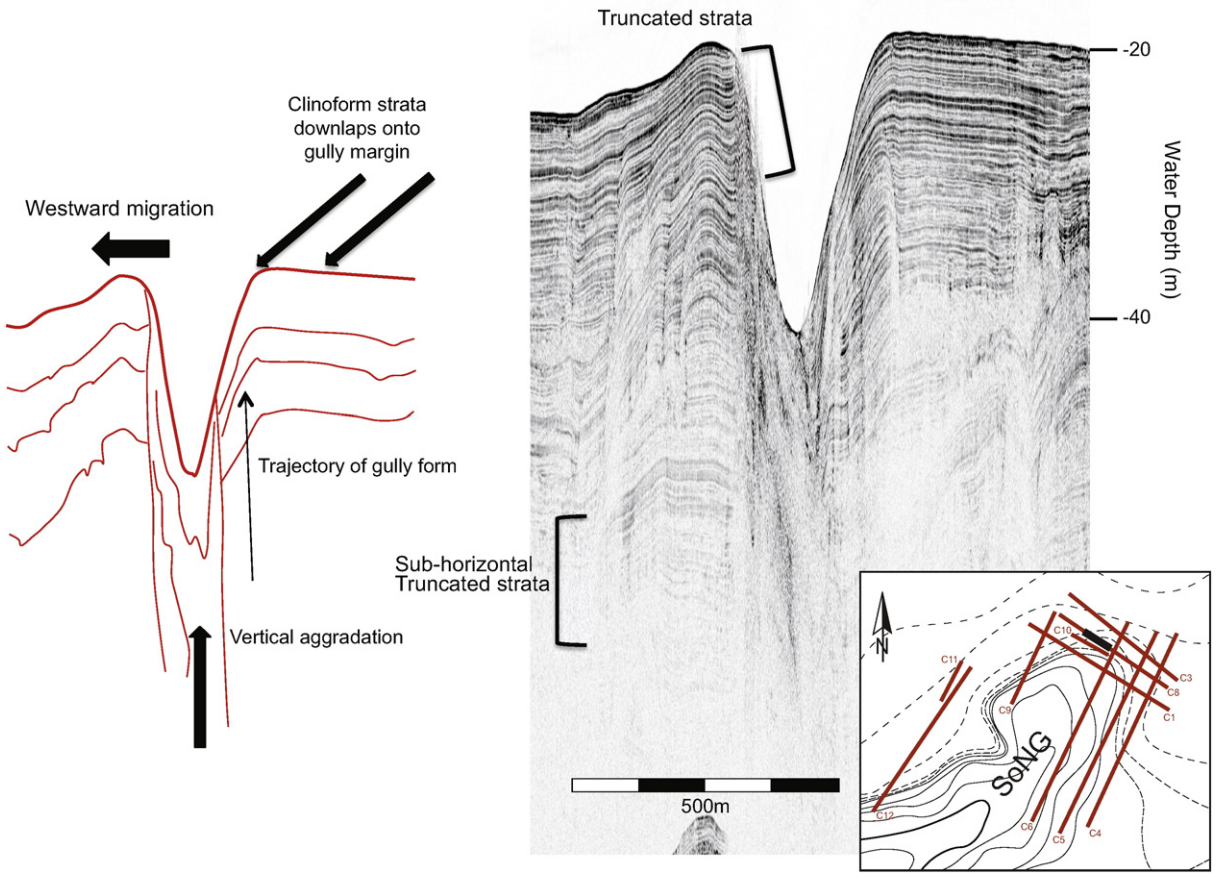

Fig. 7. Example of a vertically aggrading, laterally migrating gully form and interpreted stratigraphy sketch. Gully walls oriented towards the clinoform (on the right in this image) contain draping strata that are laterally continuous with clinoform beds, resulting in a more gently (<3°) sloping wall angle. The wall opposite the clinoform is more steeply dipping, and contains laterally truncated strata. The figure also shows gully form in the subsurface bounded by parallel bedding on both sides, suggesting that the processes maintaining the gully forms have been consistent through time. Location of the sonar line fragment is indicated on the inset map with a bold line.

removed in each valley system was obtained by summing their respective segment volumes. Volume was not calculated where there are gaps between the 2007 and 2008 data sets, with the exception of sonar line C10 and one cross line that is a part of SV-1 (Fig. 6). For these lines, a conservative estimate of failure height was made based on the measurable thickness of material removed on adjacent sonar lines within the same valley systems. Additional volume calculations were included for two failures on lines C8 and C1 (Fig. 6) that are not a part of the five main valley systems. The latter two failures appeared to have minimal runout distances and their length was taken to be 85% of the total distance to the next nearest down-canyon lines, which did not contain evidence of change between 2007 and 2008.

The calculated volume of material displaced by Cyclone Sidr is 385×10^6 m^3, equivalent to a mass failure of 578×10^6 tonnes of sediment (Table 3). While the uncertainty of this calculation is difficult to quantify due to the distance between lines in our sonar survey, the value represents a minimum because it excludes material displaced by mass flows or failures not captured in the sonar survey. Compared to previous budget estimates of annual sedimentation to the *entire* canyon (300×10^6 tonnes year^{-1}, based on sedimentation rates of up to 50 cm year^{-1} determined through ^{137}Cs and ^{228}Ra-dating of cores taken on the upper canyon floor; Michels et al., 1998) these failures compare to about two years worth of average canyon sedimentation, or 58% of the entire annual discharge for the GBM river system. Thus, a 1–3 year recurrence interval for such events would be sufficient to maintain a steady-state balance between sediment deposition in the canyon head and its subsequent export to the lower canyon system. Such a recurrence interval is also consistent with the frequency of tropical storms striking the Bengal margin, which has historically been 2–3 events annually, not all of which would of course directly impact the SoNG or be of sufficient magnitude to induce failures. Other sediment budget calculations based on a mean sedimentation rate of 20 cm year^{-1} suggest the upper canyon may store only 90×10^6 tonnes year^{-1} of sediment annually (Michels et al., 2003), in which case the 2007 failures may represent as much as 6.4 years of sediment deposition in the upper canyon.

Comparing these possible rates with the historical record, the acoustic data in this study show evidence for up to three major failure sequences impacting the SoNG canyon head over the past few hundred years (e.g., T1, T2 and T3 in Fig. 5). Based on sedimentation rates from this area of the canyon (Michels et al., 2003) and the maximum depth of observable failure scars, these values yield a maximum recurrence interval of ≤100 years for the return of a storm event of similar magnitude to Cyclone Sidr. Indeed, the relative ages of transparent units are estimated to have formed between 800 and 266 (T1), 400 and 133 (T2) and 300 and 100 (T3) years before present, respectively. This supports a centennial-scale recurrence interval of large storms capable of triggering mass failures at the SoNG canyon head. This also assumes that the buried failures were caused by storms. Earthquakes within the tectonically active Bengal Basin have been identified as another potential trigger for major seabed failure. For instance, Palamenghi et al. (2011) correlated a similar trio of transparent units on the subaqueous delta to major earthquakes in years 1762, 1897, and 1950, determined by comparing their acoustic survey data to ^{137}Cs sediment accumulation

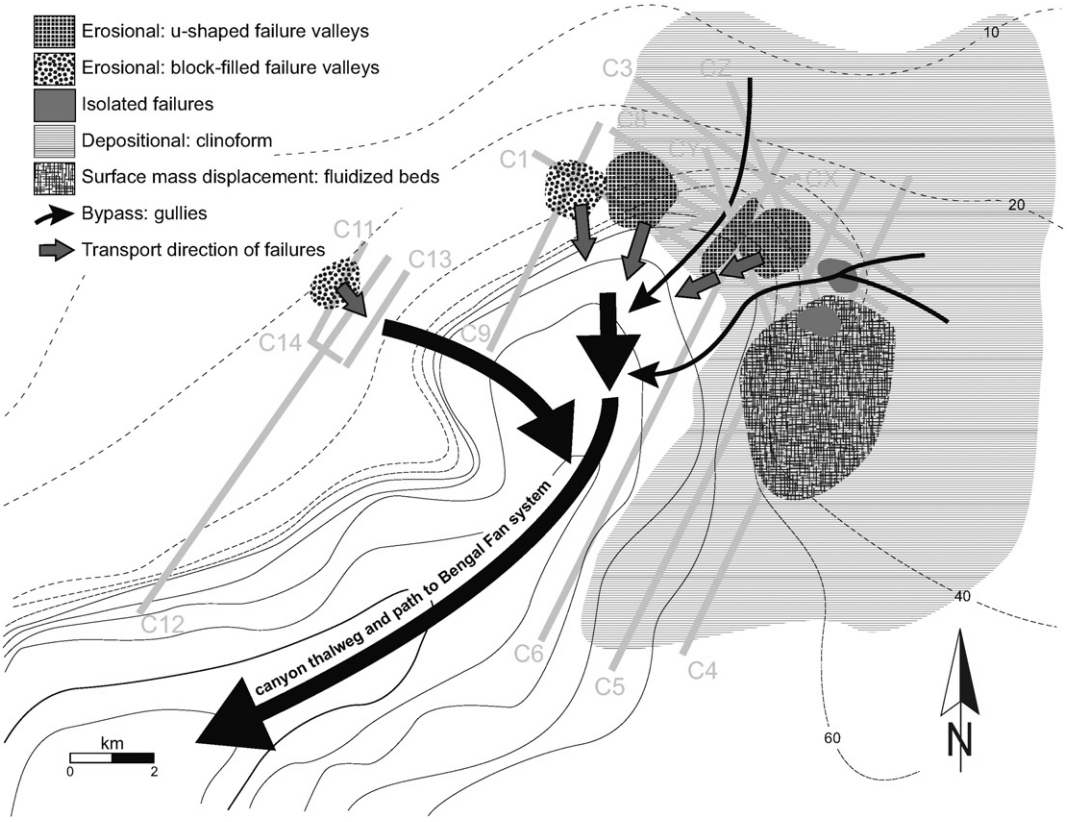

Fig. 8. Cartoon illustrating the extent and overlap of erosional, depositional and bypass features around the canyon head and where they appear on the chirp sonar survey.

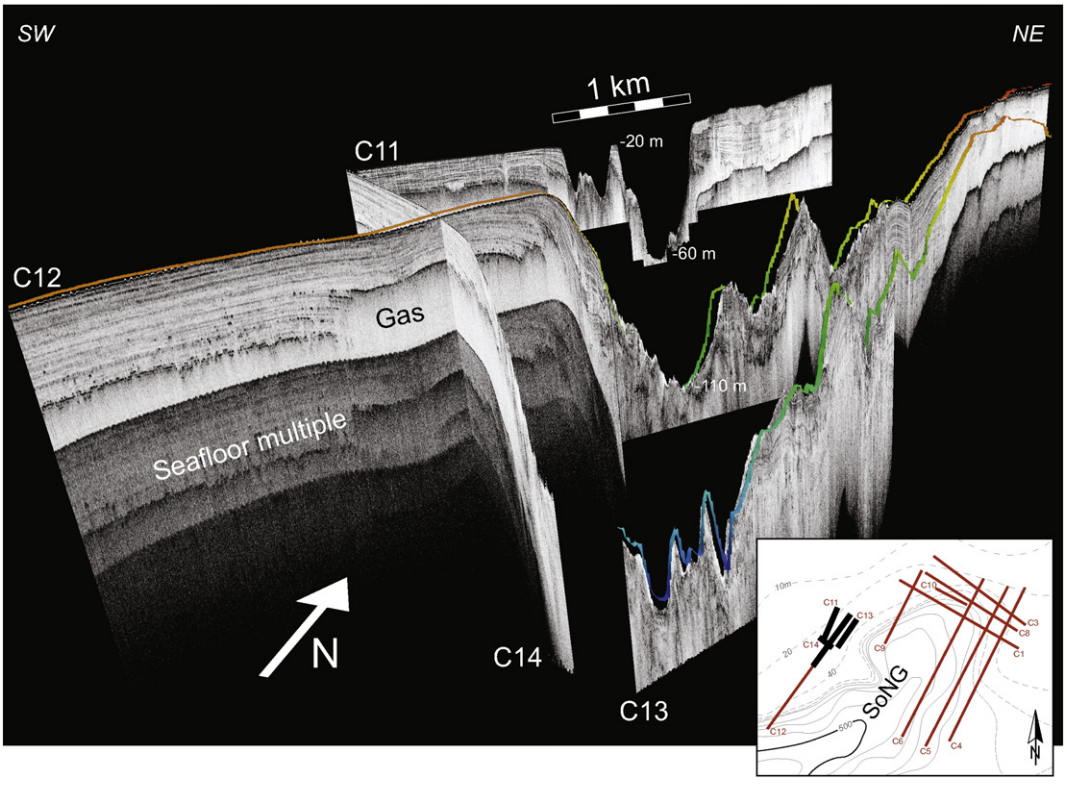

Fig. 9. Fledermaus fence image of the western canyon edge and the WSV-5 failure valley system truncating parallel strata on the western (Indian) shelf. The uppermost line in the image (C11) is the largest Sidr-related failure captured in the chirp sonar data. Comparisons of the lowermost line (C13) in pre- and post-storm images indicate ~5 m of new material was added to the seafloor. The new material consisted of acoustically transparent material that conformed to the underlying topography. Locations of the sonar line sections are indicated on the inset map with bold lines.

Table 2
Dimensions of failure valley segments used to calculate the volume of material removed by Sidr.

Failure valley	Valley segment length (m)	Thickness of failed material (m)	Width (m)	Volume of failed material per valley segment (m^3)	Total volume removed (m^3)
SV-1					
C1	900	30	1471	3.12E + 07	
ne line	2000	20	2642	8.30E + 07	1.14E + 08
SV-2					
C10	1400	10	1800	1.98E + 07	
C1	1700	8	1229	1.31E + 07	3.29E + 07
SV-3					
C8	1000	17	750	1.00E + 07	
C10	1400	15	916	1.51E + 07	
C1	1500	17	1000	2.00E + 07	
Below C1	1300	10	1800	1.84E + 07	6.35E + 07
SV-4					
C8	1300	14	2270	3.24E + 07	
C10	1800	10	1657	2.34E + 07	5.59E + 07
WSV-5					
C11	2000	40	1090	6.85E + 07	6.85E + 07
add'l failures					
C8	1500	25	1500	4.42E + 07	4.42E + 07
C1	1000	15	500	5.89E + 06	5.89E + 06
				Total	3.85E + 08

rates measured on the delta foresets by Michels et al. (1998). However, there are many fewer failures recorded in the sub-surface than there are storms or earthquakes occurring in the Bay of Bengal (Kudrass et al., 1998). Therefore the patterns observed here are consistent with larger, less frequent events that may include intense, direct storm strikes and large magnitude earthquakes.

Overall, the range of mass balance estimates above constrain the total mass mobilized by Cyclone Sidr in the SoNG to be equivalent to ~2–20 years of sedimentation at the canyon head. In sum, results of this research suggest that the balance of sediment flux into and out of the canyon during the Holocene has been maintained by recurrent mass failures on the time scale of 10–100 years. Storms of Cyclone Sidr's magnitude are known to have occurred historically in the Bay of Bengal every 3–30 years (Alam et al., 2003). Assuming that large storms track near the SoNG canyon head once a decade, it is suggested that mass failure due to storms is the principal mechanism maintaining the upper canyon head despite extremely high sedimentation rates.

6. Conclusions

The results of this study illustrate that sediment transport linking the widely-separated GBM river mouth and canyon head occurs via three principal mechanisms: 1) rapid progradation of the clinoform foresets into the eastern and northern canyon head; 2) erosion from mass wasting in failure valleys that crosscut the clinoform, and 3) funneling of sediment gravity flows from the inner shelf into the canyon via bypass gully systems. The morphologic features representing each of these processes are superimposed in the SoNG canyon head and reflect the simultaneous but largely separate occurrence of deposition (clinoform), bypass (gullies), and erosion (valleys). This provides fresh insight about the processes governing sediment transport and stability of the canyon head, whereby high rates of sedimentation are balanced by both mass failures and bypass mechanisms that transport material down-canyon. The rapid infilling and subsequent down-canyon removal of sediment stored at the SoNG canyon head has allowed the canyon to maintain its position on the shelf since the mid-Holocene. As seen in this study, individual storm events, as well as earthquakes, can generate widespread mass failures on the Bengal margin that can displace years to decades' worth of river sediment sequestered at the canyon head. However, more work is needed to quantify the overall residence time of sediment transported from the upper SoNG canyon head to the active channel-levee system of the Bengal Fan.

Table 3
Results of failure volume calculations based on a sediment bulk density of 1.5 g cm^{-3}.[1]

Total volume displaced (m^3)	3.85E + 08
Total mass displaced (tonne)	5.78E + 08
Years of total annual SoNG input removed by Sidr-related failures	>1.93
Fraction of total annual GB sediment load displaced by Sidr	0.58

[1] Although the mass of sediment annually bypassing the shelf to the canyon head is estimated at ~200×10^6 tonnes, the earlier published estimates of ~300×10^6 t $year^{-1}$ will be used to calculate the volume of material displaced by the Cyclone Sidr. This allows the current sediment budget to be placed in the context of the previously published sediment budgets for the GBM system.

Acknowledgments

We would like to thank Emadadul Haque (Bangladesh Inland Waterways Transportation Authority), the crew of the R/V *Dishari*, and Mohammad "Apu" Ullah for their assistance with data collection. The MODIS image in Fig. 1 was retrieved from https://lpdaac.usgs.gov, maintained by the NASA EOSDIS Land Processes Distributed Active Archive Center (LP DAAC) at the USGS/Earth Resources Observation and Science (EROS) Center, Sioux Falls, South Dakota. The data product for the image was provided by NASA. Early versions of this manuscript were greatly improved with helpful comments from Chris Jenkins and two anonymous reviewers. The research was funded though National Science Foundation grant OCE-0630595.

References

Alam, M.M., Hossain, M.A., Shafee, S., 2003. Frequency of Bay of Bengal cyclonic storms and depressions crossing different coastal zones. Int. J. Climatol. 23, 1119–1125.
Allison, M.A., 1998. Geologic framework and environmental status of the Ganges–Brahmaputra Delta. J. Coast. Res. 14 (3), 826–836.
Allison, M.A., Kepple, E., 2001. Modern sediment supply to the lower delta plain of the Ganges–Brahmaputra River in Bangladesh. Geo-Mar. Lett. 21 (2), 66–74.
Allison, M.A., Khan, S.R., Goodbred, S.L., Kuehl, S.A., 2003. Stratigraphic evolution of the late Holocene Ganges–Brahmaputra lower delta plain. Sediment. Geol. 155, 317–342.

Barua, D.P., 1990. Suspended sediment movement in the estuary of the Ganges–Brahmaputra–Meghna River system. Mar. Geol. 91, 243–253.
Barua, D.K., Kuehl, S.A., Miller, R.L., Moore, W.S., 1994. Suspended sediment distribution and residual transport in the coastal ocean off of the Ganges–Brahmaputra river mouth. Mar. Geol. 120, 41–61.
Coleman, J.M., 1969. Brahmaputra River: channel processes and sedimentation. Sediment. Geol. 3, 129–239.
Flood, R.D., Piper, D.J.W., Klaus, A., Peterson, L.C. (Eds.), 1997. Proceedings of the ocean drilling program, Scientific Results vol. 155.
Gibling, M.R., 2006. Width and thickness of fluvial channel bodies and valley fills in the geological record: a literature compilation and classification. J. Sediment. Res. 76 (5), 731–770.
Goodbred, S.L., Kuehl, S.A., 1998. Floodplain processes in the Bengal Basin and the storage of Ganges–Brahmaputra river sediment: an accretion study using ^{137}Cs and ^{210}Pb geochronology. Sediment. Geol. 121, 239–258.
Goodbred, S.L., Kuehl, S.A., 1999. Holocene and modern sediment budgets for the Ganges–Brahmaputra river system: evidence for highstand dispersal to flood-plain, shelf, and deep-sea depocenters. Geology 27 (6), 559–562.
Goodbred, S.L., Kuehl, S.A., 2000. The significance of large sediment supply, active tectonism, and eustacy on margin sequence development: late Quaternary stratigraphy and evolution of the Ganges–Brahmaputra delta. Sediment. Geol. 133, 227–248.
Goodbred, S.L., Paolo, P.M., Ullah, MdS., Pate, R.D., Khan, S.R., Kuehl, S.A., Singh, S.K., Rahaman, W., 2014. Piecing together the Ganges–Brahmaputra–Meghna river delta: application of Sr sediment geochemistry to reconstruct river-channel histories and Holocene delta evolution. Geol. Soc. Am. Bull B30965-1.
Hampton, M., Lee, H.J., Locat, J., 1996. Submarine landslides. Rev. Geophys. 34, 33–59.
Harris, P.T., Whiteway, T., 2011. Global distribution of large submarine canyons: geomorphic differences between active and passive continental margins. Mar. Geol. 285 (1–4), 69–86.
Harris, P.T., Baker, E.K., Cole, A.R., Short, S.A., 1993. A preliminary study of sedimentation in the tidally dominated Fly River Delta, Gulf of Papua. Cont. Shelf Res. 13 (4), 441–472.
Hübscher, C., Breitzke, M., Michels, K., Kudrass, H.R., Spiess, V., Wiedicke, M., 1998. Late Quaternary seismic stratigraphy of the eastern Bengal Shelf. Mar. Geophys. Res. 20 (1), 57–71.
Huh, C.A., Liu, J.T., Lin, H.L., Xu, J.P., 2009. Tidal and flood signatures of settling particles in the Gaoping submarine canyon (SW Taiwan) revealed from radionuclide and flow measurements. Mar. Geol. 267 (1), 8–17.
Islam, M.R., Begum, S.F., Yamaguchi, Y., Ogawa, K., 2002. Distribution of suspended sediment in the coastal sea off the Ganges–Brahmaputra River mouth; observation from TM data. J. Mar. Syst. 32, 307–321.
Izumi, N., 2004. The formation of submarine gullies by turbidity currents. J. Geophys. Res. 109 (C3), C03048.
Kineke, G.C., Sternberg, R.W., Trowbridge, J.H., Geyer, W.R., 1996. Fluid-mud processes on the Amazon continental shelf. Cont. Shelf Res. 16 (5/6), 667–696.
Kineke, G.C., Woolfe, K.J., Kuehl, S.A., Milliman, J.D., Dellapenna, T.M., Purdon, R.G., 2000. Sediment export from the Sepik River, Papua New Guinea: evidence for a divergent sediment plume. Cont. Shelf Res. 20 (16), 2239–2266.
Kolla, V., Coumes, F., 1987. Morphology, internal structure, seismic stratigraphy, and sedimentation of Indus Fan. AAPG Bull. 71 (6), 650–677.
Kolla, V., Perlmutter, M.A., 1993. Timing of turbidite sedimentation on the Mississippi Fan. AAPG Bull. 77 (7), 1129–1141.
Kottke, B., Schwenk, T., Breitzke, M., Wiedicke, M., Kudrass, H.R., Spiess, V., 2003. Acoustic facies and depositional processes in the upper submarine canyon Swatch of No Ground (Bay of Bengal). Deep-Sea Res. II 50, 979–1001.
Kudrass, H.R., Michels, K.H., Wiedicke, M., Suckow, A., 1998. Cyclones and tides as feeders of a submarine canyon off Bangladesh. Geology 26, 715–717.
Kuehl, S.A., Brunskill, G.J., Burns, K., Fugate, D., Kniskern, T., Meneghini, L., 2004. Nature of sediment dispersal off the Sepik River, Papua New Guinea: preliminary sediment budget and implications for margin processes. Cont. Shelf Res. 24, 2417–2429.
Kuehl, S.A., Hariu, T.M., Moore, W.S., 1989. Shelf sedimentation off the Ganges–Brahamputra river system: evidence for sediment bypassing to the Bengal fan. Geology 17, 1132–1135.
Kuehl, S.A., Levy, B.M., Moore, W.S., Allison, M.A., 1997. Subaqueous delta of the Ganges–Brahmaputra river system. Mar. Geol. 144, 81–96.
Maillet, G.M., Vella, C., Berne, S., Friend, P.L., Amos, C.L., Fleury, T.J., Normand, A., 2006. Morphological changes and sedimentary processes induced by the December 2003 flood event at the present mouth of the Grand Rhône River (southern France). Mar. Geol. 234, 159–177.
Michels, K.H., Kudrass, H.R., Hübscher, C., Suckow, A., Wiedicke, M., 1998. The submarine delta of the Ganges–Brahmaputra: cyclone dominated sedimentation patterns. Mar. Geol. 149, 133–154.
Michels, K.H., Suckow, A., Breitzke, M., Kudrass, H.R., Kottke, B., 2003. Sediment transport in the shelf canyon "Swatch of No Ground" (Bay of Bengal). Deep-Sea Res. II 50, 1003–1022.
Milliman, J.D., Summerhayes, C.P., Barretto, H.T., 1975. Quaternary sedimentation on the Amazon continental margin: a model. Geol. Soc. Am. Bull. 86, 610–614.
Moscardelli, L., Wood, L., Mann, P., 2006. Mass transport complexes and associated processes in the offshore area of Trinidad and Venezuela. AAPG Bull. 90 (7), 1059–1088.
Mullenbach, B.L., Nittrouer, C.A., 2000. Rapid deposition of fluvial sediment in the Eel Canyon, northern California. Cont. Shelf Res. 20 (16), 2191–2212.
Mullenbach, B.L., Nittrouer, C.A., Puig, P., Orange, D.L., 2004. Sediment deposition in a modern submarine canyon: Eel Canyon, northern California. Mar. Geol. 211 (1), 101–119.
Palamenghi, L., Schwenk, T., Spiess, V., Kudrasss, H.R., 2011. Seismostratigraphic analysis with centennial to decadal time resolution of the sediment sink in the Ganges-Brahmaputra subaqueous delta. Cont. Shelf Res. 31, 712–730.
Palanques, A., Durrieu de Madron, X., Puig, P., Fabres, J., Guillén, J., Calafat, A., Canals, M., Heussner, S., Bonnin, J., 2006. Suspended sediment fluxes and transport processes in the Gulf of Lions submarine canyons. The role of storms and dense water cascading. Mar. Geol. 234 (1), 43–61.
Prior, D.B., Yang, Z.-S., Bornhold, B.D., Keller, G.H., Lu, N.Z., Wiseman Jr., W.J., Wright, L.D., Zhang, J., 1986. Active slope failure, sediment collapse, and silt flows on the modern subaqueous Huanghe (Yellow River) delta. Geo-Mar. Lett. 6, 85–95.
Popescu, I., Lericolais, G., Panin, N., Normand, A., Dinu, C., Le Drezen, E., 2004. The Danube submarine canyon (Black Sea): morphology and sedimentary processes. Mar. Geol. 206, 249–265.
Puig, P., Ogston, A.S., Mullenbach, B.L., Nittrouer, C.A., Parsons, J.D., Sternberg, R.W., 2004. Storm-induced sediment gravity flows at the head of the Eel submarine canyon, northern California margin. J. Geophys. Res. 109 (C3), C03019.
Puig, P., Palanques, A., Martín, J., 2014. Contemporary sediment-transport processes in submarine canyons. Ann. Rev. Mar. Sci. 6, 53–77.
Rogers, K.G., Goodbred, S.L., 2010. Mass failures associated with the passage of a large tropical cyclone over the Swatch of No Ground submarine canyon (Bay of Bengal). Geology 38 (11), 1051–1054.
Rogers, K.G., Goodbred, S.L., Mondal, D.R., 2013. Monsoon sedimentation on the 'abandoned' tide-influenced Ganges–Brahmaputra delta plain. Estuar. Coast. Shelf Sci. 131, 297–309.
Savoye, B., Babonneau, N., Dennielou, B., Bez, M., 2009. Geological overview of the Angola–Congo margin, the Congo deep-sea fan and its submarine valleys. Deep-Sea Res. II Top. Stud. Oceanogr. 56 (23), 2169–2182.
Sengupta, R., Basu, P.C., Bandyopadhyay, R.R., Bandyopadhyay, A., Rakshit, S., Sharma, B., 1992. Sediments in the continental shelf in and around the Swatch of No Ground. Geol. Surv. India Spec. Publ. 29, 201–207.
Smith, D.P., Ruiz, G., Kvitek, R., Iampietro, P.J., 2005. Semiannual patterns of erosion and deposition in upper Monterey Canyon from serial multibeam bathymetry. Geol. Soc. Am. Bull. 117 (9–10), 1123–1133.
Spinelli, G.A., Field, M.E., 2001. Evolution of continental slope gullies on the northern California margin. J. Sediment. Res. 71 (2), 237–245.
Sternberg, R.W., Cacchione, D.A., Paulson, B., Kineke, G.C., Drake, D.E., 1996. Observations of sediment transport on the Amazon subaqueous delta. Cont. Shelf Res. 20, 2113–2140.
Straub, K.M., Mohrig, D., 2009. Constructional canyons built by sheet-like turbidity currents: observations from offshore Brunei Darussalam. J. Sediment. Res. 79, 24–39.
Syvitski, J.P.M., Burrell, D.C., Skei, J.M., 1987. Fjords: processes and products. Springer-Verlag, New York, p. 379.
Talling, P.J., 2014. On the triggers, resulting flow types and frequencies of subaqueous sediment density flows in different settings. Mar. Geol. 352, 155–182.
Twichell, D.C., Roberts, D.G., 1982. Morphology, distribution, and development of submarine canyons on the Unite States Atlantic continental slope between Hudson and Baltimore Canyons. Geology 10 (8), 408–412.
Trincardi, F., Cattaneo, A., Correggiari, A., Ridente, D., 2004. Evidence of soft sediment deformation, fluid escape, sediment failure and regional weak layers within the late Quaternary mud deposits of the Adriatic Sea. Mar. Geol. 213, 91–119.
Weber, M.E., Wiedicke, M.H., Kudrass, H.R., Hübscher, C., Erlenkeuser, H., 1997. Active growth of the Bengal Fan during sea-level rise and highstand. Geology 25 (4), 315–318.
Wright, L.D., Friedrichs, C.T., 2006. Gravity-driven sediment transport on continental shelves: a status report. Cont. Shelf Res. 26, 2092–2107.